Inorganic Chemistry
Cite This: Inorg. Chem. XXXX, XXX, XXX−XXX
Article
pubs.acs.org/IC

Metal−Organic Framework Based on Heptanuclear Cu−O Clusters and Its Application as a Recyclable Photocatalyst for Stepwise Selective Catalysis

Jie Zhou,[†] Xu Huang-Fu,[†] Yang-Ying Huang,[†] Chu-Ning Cao,[†] Jie Han,[‡] Xiao-Li Zhao,*[,§] and Xu-Dong Chen*[,†]

[†]Jiangsu Key Laboratory of Biofunctional Materials and Jiangsu Collaborative Innovation Center of Biomedical Functional Materials, School of Chemistry and Materials Science, Nanjing Normal University, Nanjing 210023, China

[‡]School of Science & Technology, The Open University of Hong Kong, Kowloon, Hong Kong SAR, China

[§]Shanghai Key Laboratory of Green Chemistry and Chemical Processes, Department of Chemistry, East China Normal University, Shanghai 200062, China

Supporting Information

ABSTRACT: Visible-light driven photoreactions using metal−organic frameworks (MOFs) as catalysts are promising with regard to their environmental friendly features such as the use of renewable and sustainable energy of visible light and potential catalyst recyclability. To develop potential heterogeneous photocatalysts, a family of three copper(II) coordination polymers bearing different Cu−O assemblies have been synthesized with the ligand 4,4′-disulfo-[1,1′-biphenyl]-2,2′-dicarboxylate acid (H_4DSDC), namely, $\{[Cu_7(DSDC)_2(OH)_6(H_2O)_{10}]\cdot xH_2O\}_n$ (**1**), $\{[Cu_4(DSDC)(4,4'\text{-bpy})_2(OH)_4]\cdot 2H_2O\}_n$ (**2**), and $\{Cu_2(DSDC)(phen)_2(H_2O)_2\}_n$ (**3**) (4,4′-bpy = 4,4′-bipyridine and phen = 1,10-phenanthroline). Complex **1** represents a metal−organic framework featuring a NbO type topology constructed from the infinite linkage of heptanuclear $[Cu_7(\mu_3\text{-}OH)_6(H_2O)_{10}]^{8+}$ clusters by deprotonated $DSDC^{4-}$ ligands, comprising one-dimensional hexagonal channels of a diameter around 11 Å that are filled with water molecules. The infinite waving $\{[Cu_2(OH)_2]^{2+}\}_n$ ladderlike chains in complex **2** are bridged by $DSDC^{4-}$ and 4,4′-bpy ligands into a three-dimensional framework. A two-dimensional layered structure is formed in complex **3** due to the existence of terminal phenanthroline ligands. All of the coordination polymers **1**−**3** are able to catalyze the visible-light driven oxidation of alcohols at mild conditions using hydrogen peroxide as an oxidant, in which complex **1** demonstrates satisfactory efficiency. Significantly for this photoreaction catalyzed by **1**, the extent of oxidation over aryl primary alcohols is fully controllable with time-resolved product selectivity, giving either corresponding aldehydes or carboxylate acids in good yields. It is also remarkable that the photocatalyst could be recovered almost quantitatively on completion of the catalytic cycle without any structure change, and could be recycled for catalytic use for at least five cycles with constant efficiency. This photocatalyst with time-resolved selectivity for different products may provide new insight into the design and development of novel catalytic systems.

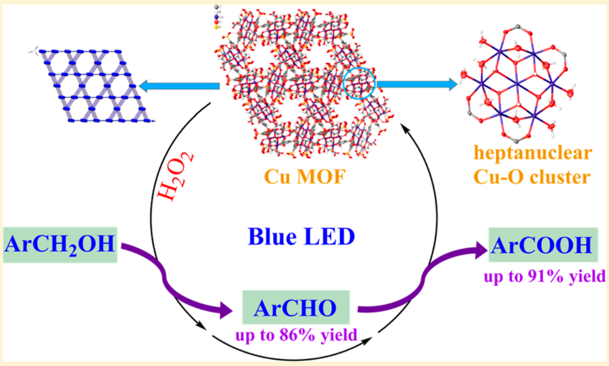

INTRODUCTION

The polymeric coordination of metal cations and organic ligands into highly ordered structures provides us with a promising category of functional materials, and the so-called coordination polymers (e.g., metal−organic frameworks) have wide applications in many fields such as proton conduction,[1−5] gas storage,[6−10] separation,[11−18] photoluminescence,[19−23] organic catalysis,[24−28] and so on. Their typical features, such as flexible coordination geometry, facile functionalization through design and modification, easy isolation due to poor solubility in common solvents, and potentially high atom economy, make them perfect candidates as heterogeneous catalysts.

Photocatalysis utilizing the renewable and sustainable energy of visible light holds intrinsic advantages in the aspects of both mild reaction conditions and product selectivity and hence is growing into a powerful tool in organic synthesis.[29−32] Metal (Ru^{II}, Ir^{III}, Re^{I}, and Os^{II}) polypyridine complexes and organic dyes are two typical categories of photocatalysts that have attracted intense research interests.[33−37] Metal−organic frameworks (MOFs) have demonstrated their success as heterogeneous catalysts in organic transformations, whereas their applications in heterogeneous photocatalysis have been scarce.[24,38−40] It is highly desirable to develop efficient heterogeneous photocatalysts with high catalytic activity, good selectivity, and perfect recyclability in terms of green

Received: July 13, 2019

DOI: 10.1021/acs.inorgchem.9b02084
Inorg. Chem. XXXX, XXX, XXX−XXX

chemistry.[41] Therefore, our attention has been focused on the development of novel coordination polymers as efficient heterogeneous photocatalysts.

Coordination complexes comprising Cu−O clusters have been widely used as catalysts in molecular polymerization and oxidation reactions.[42−44] According to the feature that carboxylate groups would ligate with Cu(II) cations under basic conditions to generate Cu−O cluster structures,[42,45,46] the ligand 4,4′-disulfo-[1,1′-biphenyl]-2,2′-dicarboxylate acid has therefore been synthesized, which bears both carboxylate and sulfonate groups. The expectation is that rich coordinating groups would allow not only the formation of cluster structures but also infinite linkage of such clusters into a polymeric framework, which would qualify as a good candidate for heterogeneous catalysis. On the basis of this ligand, and in certain cases together with auxiliary ligands, a series of coordination polymers bearing different Cu−O cluster structures have been synthesized, and their applications in catalyzing oxidation of primary aryl alcohols using hydrogen peroxide as an oxidant upon irradiation of visible light at room temperature have thus been examined.

Remarkably, this photocatalyst could be recovered almost quantitatively on completion of the reaction without any structure change, which proved capable of recycled use for at least five catalytic cycles with constant activity. With aryl primary alcohols as the substrate, the oxidation product proved to be either aldehyde or carboxylic acid, indicating a unique time-resolved oxidation process with a good product selectivity. This type of restorable and recyclable photocatalyst capable of selective catalysis over successive reactions may shed light on the design and development of novel heterogeneous catalysts toward challenging organic reactions.

■ EXPERIMENTAL SECTION

General Materials and Measurements. All reagents and solvents were purchased from commercial sources and used without further purification. The ligand H_4DSDC was synthesized using a modified procedure as reported.[47,48] Possible Cu(II) cations leaching in reaction solution were measured on a PLASMASPEC (I) ICP atomic emission spectrometer. Thermal analyses were carried out on a Mettler-Toledo TGA/DSC STARe system in the temperature range from room temperature to 800 °C with a heating rate of 10 $°C\cdot min^{-1}$, under a nitrogen flow. Infrared spectra were recorded on a VECTOR 22 spectrometer and an Alpha Centaur Fourier transform infrared (FTIR) spectrometer with pressed KBr pellets in the range 4000−400 cm^{-1}. Powder X-ray diffraction (PXRD) was performed using a MiniFlex 600 X-ray powder diffractometer equipped with a Cu sealed tube (λ = 1.54178 Å) at 40 kV and 40 mA. ^1H and ^{13}C NMR spectra were obtained on a Bruker 400 MHz spectrometer.

Synthesis of 4,4′-Disulfo-[1,1′-biphenyl]-2,2′-dicarboxylate acid (H_4DSDC). 9,10-Phenanthraquinone-2,7-disulfonic acid (7.36 g) and acetic acid (15.0 mL) were placed in a two-necked flask, and the mixture was heated to 85 °C while stirring. Then 40.0 mL of 30% H_2O_2 solution was added dropwise into the mixture over a period of 2 h. After stirring at 80 °C for another 12 h, the mixture was cooled to room temperature and concentrated on a rotavapor. The product was obtained at 81% yield as a white powder upon the addition of acetonitrile into the concentrated solution, which was collected by filtration and dried at ambient temperature. ^1H NMR (400 MHz, D_2O, δ, ppm): 8.34 (s, 2H), 7.99 (d, 2H), 7.44 (dd, 2H). ^{13}C NMR (400 MHz, D_2O, δ, ppm): 169.44, 144.46, 142.12, 130.99, 129.79, 128.91, 126.90.

Synthesis of $\{[Cu_7(DSDC)_2(OH)_6(H_2O)_{10}]\cdot xH_2O\}_n$ (**1**). A mixture of $Cu(NO_3)_2\cdot 3H_2O$ (24.2 mg, 0.1 mmol) and H_4DSDC (20.1 mg, 0.05 mmol) was dissolved into a mixed solvent of dimethylacetamide/water (2.0/1.0 mL) in a 10 mL glass vial. After the addition of 1.0 mL of 0.2 M NaOH solution, the vessel was sealed with a cap and then heated to 130 °C. The reaction mixture was held at 130 °C for 30 min and cooled to room temperature slowly to generate light blue crystals, which were collected by filtration, washed with CH_3OH, and dried at ambient temperature. Yield: 60% based on H_4DSDC. Elemental analysis for $C_{14}H_{19}Cu_{3.5}O_{18}S_2$, calcd (%): C, 22.07; H, 2.51. Found: C, 22.10; H, 2.46. IR spectrum (cm^{-1}, KBr pellet): 3411 (s), 1596 (s), 1543 (s), 1411 (s), 1367 (m), 1217 (m), 1164 (s), 1147 (m), 1093 (m), 1041 (s), 996 (m), 828 (w), 802 (w), 785 (w), 757 (w), 670 (m), 617 (m), 572 (s), 554 (s), 476 (s).

Synthesis of $\{[Cu_4(DSDC)(4,4'\text{-}bpy)_2(OH)_4]\cdot 2H_2O\}_n$ (**2**). A mixture of $Cu(NO_3)_2\cdot 3H_2O$ (24.2 mg, 0.1 mmol), 4,4′-bipyridine (15.6 mg, 0.1 mmol), and H_4DSDC (20.1 mg, 0.05 mmol) was dissolved into a mixed solvent of dimethylacetamide/water (3.0/1.0 mL) in a 10 mL glass vial. After the addition of 1.0 mL of 0.2 M NaOH solution, the vessel was sealed with a cap and then heated to 130 °C. The reaction mixture was held at 130 °C for 12 h and cooled to room temperature slowly to give green crystals, which were collected by filtration, washed with CH_3OH, and dried at ambient temperature. Yield: 72% based on H_4DSDC. Elemental analysis for $C_{17}H_{15}Cu_2N_2O_8S$, calcd (%): C, 38.20; H, 2.83; N, 5.24. Found: C, 38.25; H, 2.78; N, 5.20. IR spectrum (cm^{-1}, KBr pellet): 3454 (m), 3102 (w), 3045 (w), 1614 (m), 1558 (s), 1422 (s), 1393 (s), 1365 (s), 1223 (s), 1195 (s), 1171 (s), 1165 (m), 1143 (m), 1120 (w), 1103 (w), 1074 (w), 1035 (s), 990 (m), 961 (w), 842 (w), 819 (s), 768 (w), 734 (w), 666 (m), 643 (m), 608 (s), 450 (s).

Synthesis of $\{Cu_2(DSDC)(phen)_2(H_2O)_2\}_n$ (**3**). $Cu(NO_3)_2\cdot 3H_2O$ (24.2 mg, 0.1 mmol), 1,10-phenanthroline (18.0 mg, 0.1 mmol), and H_4DSDC (20.1 mg, 0.05 mmol) were dissolved into a mixed solvent of dimethylformamide/water (2.0/1.0 mL) in a 10 mL glass vial. After the addition of 1.0 mL of 0.2 M NaOH solution, the vessel was sealed with a cap and then heated to 130 °C. The reaction mixture was held at 130 °C for 2 days and cooled to room temperature slowly to give navy blue crystals, which were collected by filtration, washed with CH_3OH, and dried at ambient temperature. Yield: 81% based on H_4DSDC. Elemental analysis for $C_{38}H_{26}Cu_2N_4O_{12}S_2$, calcd (%): C, 49.51; H, 2.84; N, 6.08. Found: C, 49.51; H, 2.77; N, 6.09. IR spectrum (cm^{-1}, KBr pellet): 3414 (s), 3108 (m), 3073 (m), 3057 (m), 1603 (s), 1574 (s), 1500 (m), 1467 (m), 1432 (s), 1410 (m), 1353 (s), 1120 (m), 1098 (m), 1035 (s), 990 (m), 910 (vw), 865 (vw), 836 (vw), 802 (w), 768 (s), 734 (m), 671 (m), 620 (s), 541 (w), 404 (w).

Typical Procedure for a Photocatalytic Experiment. Into a 25 mL Schlenk tube equipped with a magnetic stir bar were added the catalyst (0.04 mmol), MeCN (2.0 mL), and benzyl alcohol (0.4 mmol). After the addition of 30% hydrogen peroxide (1.2 mmol), the reaction mixture was stirred at room temperature under the irradiation of a blue LED. In one of the parallel runs, the oxidation product was isolated after 24 h. The reaction mixture was filtrated, and the filtrate was quenched by water (2.0 mL) and extracted with EtOAc (20 mL × 3). The combined organic phase was washed with brine (20 mL × 2), dried over Na_2SO_4 and $MgSO_4$, evaporated to dryness, and subjected to column chromatography (silica gel, petroleum ether/ethyl acetate) to furnish the product, which was characterized by ^1H and ^{13}C NMR to be benzaldehyde (74% yield). When benzaldehyde was not isolated and the reaction carried on for 60 successive hours, the reaction mixture was filtrated to afford a microcrystalline solid and the filtrate. The solid was washed by dichloromethane, dried in vacuum, and subjected to powder XRD analysis to prove a material identical to the fresh prepared catalyst, which was good for recycled use of the oxidation reaction. The filtrate was quenched by NaOH solution and washed by EtOAc (20 mL × 3). The aqueous phase was then acidified by concentrated hydrochloric acid to precipitate the benzoic acid, which was collected by filtration, washed with small amount of water, and dried to afford benzoic acid in 88% yield. All yields reported are based on isolated pure products and characterization was performed using ^1H and ^{13}C NMR spectroscopy (see Supporting Information for spectra).

Single-Crystal X-ray Crystallography. Single-crystal X-ray diffraction data of all three complexes were collected at 293 K using a Bruker APEX II CCD diffractometer operating at 50 kV and 30 mA using Mo Kα radiation (λ = 0.71073 Å). Data were integrated using SAINT and scaled with either a numerical or multiscan absorption correction using SADABS[49] All structures were solved by direct

Table 1. Crystallographic Data for Complexes 1−3

	1	2	3
empirical formula	$C_{14}H_{19}Cu_{3.5}O_{18}S_2$	$C_{17}H_{15}Cu_2N_2O_8S$	$C_{38}H_{26}Cu_2N_4O_{12}S_2$
Fw	761.80	534.45	921.83
crystal system	trigonal	monoclinic	orthorhombic
space group	$R\bar{3}$	$C2/c$	$Pccn$
a (Å)	31.674(4)	14.295(2)	28.604(4)
b (Å)	31.674(4)	18.460(3)	14.5604(18)
c (Å)	16.052(4)	15.322(2)	17.081(2)
α (deg)	90	90	90
β (deg)	90	115.887(2)	90
γ (deg)	120	90	90
V (Å^3)	13947(5)	3637.5(11)	7114.0(16)
Z	18	8	8
D calcd (g·cm^{-3})	1.633	1.952	1.721
μ (mm^{-1})	2.575	2.507	1.388
$F(000)$	6849	2152	3744
goodness-of-fit on F^2	1.072	1.036	1.017
$R1$,[a] $wR2$[b] [$I > 2\sigma(I)$]	0.0418, 0.1023	0.0286, 0.0702	0.0319, 0.0767
$R1$,[a] $wR2$[b] (all data)	0.0667, 0.1133	0.0362, 0.0745	0.0450, 0.0826
$(\Delta\rho)$max, $(\Delta\rho)$min (e·Å^{-3})	0.875, −0.428	0.493, −0.376	0.32, −0.36

[a] $R_1 = \sum ||F_o| - |F_c|| / \sum |F_o|$. [b] $wR_2 = \{\sum [w(F_o^2 - F_c^2)^2] / \sum [w(F_o^2)^2]\}^{1/2}$.

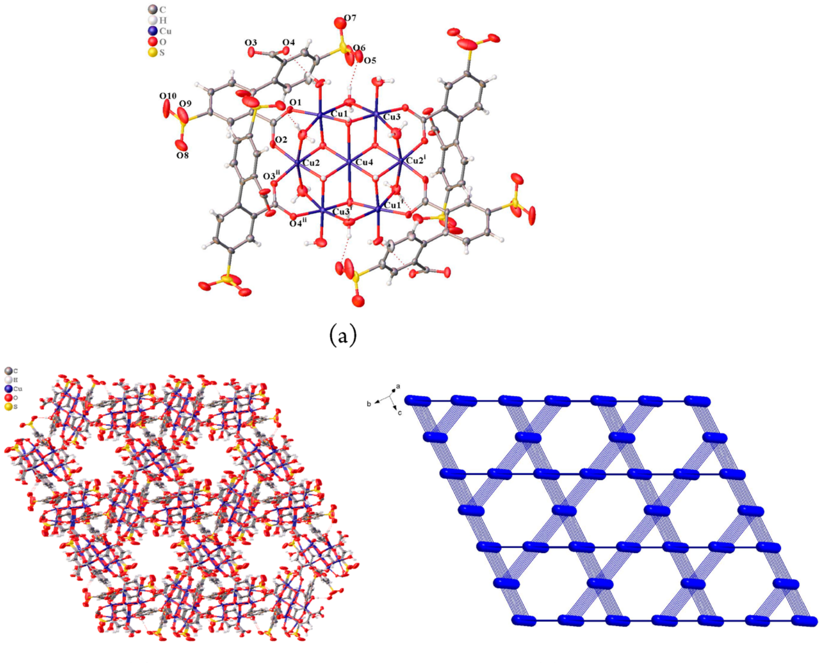

(a)

(b)

(c)

Figure 1. (a) Heptanuclear $[Cu_7(\mu_3\text{-}OH)_6(H_2O)_{10}]^{8+}$ cluster in complex **1** surrounded by $DSDC^{4-}$ ligands, showing coordination geometries of the Cu(II) centers. (b) Packing diagram of complex **1** with one-dimensional channels along the [001] direction. Disordered guest molecules are omitted for clarity. (c) Topological representation of the framework in complex **1**. The blue nodes and lines represent the $[Cu_7(\mu_3\text{-}OH)_6(H_2O)_{10}]^{8+}$ SBUs and $DSDC^{4-}$ ligands, respectively. Symmetry code: ^{i} $1 - x, 1 - y, 2 - z$; ^{ii} $1/3 - y + x, -1/3 + x, 5/3 - z$.

methods or Patterson maps[50] and refined by full-matrix least squares on F^2 using the SHELXL-2014[51] and OLEX2[52] programs. All non-hydrogen atoms were refined anisotropically. Non-water hydrogen atoms were added at calculated positions and refined using a riding model. Hydrogen atoms of water molecules and hydroxyl groups were located by difference Fourier maps and refined using a riding model at a restrained distance of 0.86 Å. The disordered water molecules in the channels of the framework in complex **1** could not be modeled very well and were treated by the SQUEEZE routine, resulting in the absence of hydrogen bonding acceptor for H5wB. For complex **2**, one of the lattice water molecules (O8) suffered from disorder, which led to uncertainty in the position. Crystallographic data of all three complexes are summarized in Table 1, and selected bond lengths and angles are listed in Table S1 in the Supporting Information.

■ RESULTS AND DISCUSSION

Syntheses and Structures of Candidate Photocatalysts. Versatile coordination groups in the designed $DSDC^{4-}$ ligand dictate rich potential coordination modes that may facilitate the formation of versatile Cu−O moieties and lead to various polymeric complexes. As for a systematic comparison,

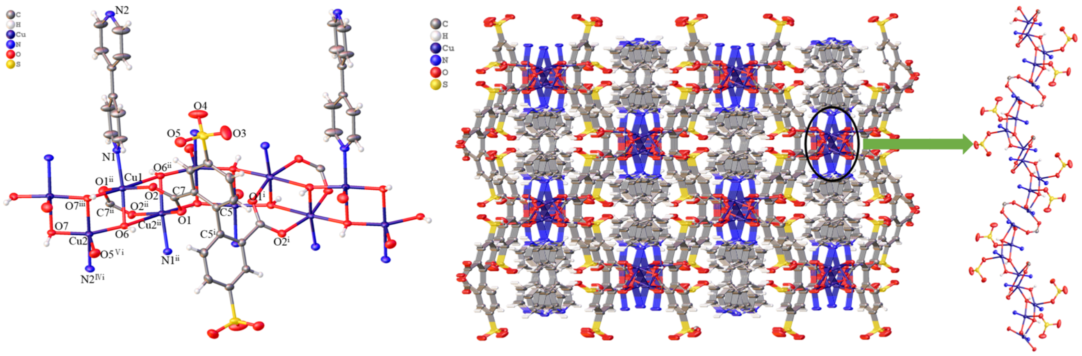

(a) (b)

Figure 2. (a) One-dimensional ladderlike belt in complex **2**, showing the coordination geometry of metal centers and bridging mode of the $DSDC^{4-}$ ligand. (b) Three-dimensional framework in complex **2** assembled from one-dimensional belts. Symmetry codes: ^{i} $-x, +y, 3/2 - z$; ^{ii} $-x, 1 - y, 1 - z$; ^{iii} $-x, +y, 1/2 - z$; ^{iv} $-1 + x, 1 - y, -1/2 + z$; ^{v} $-1/2 + x, 3/2 - y, -1/2 + z$.

complexes **2** and **3** with additional different auxiliary ligands have also been synthesized and their photocatalytic activities have been studied and compared with that of complex **1** regarding the same reaction. The selection of the auxiliary ligands is based on the consideration of either good connectivity for better stability and limited solubility or the potential of increasing photosensitivity of the metal complex for better photocatalytic activity. All three Cu(II) complexes synthesized are revealed to be polymeric according to the X-ray single-crystal structure analyses, demonstrating poor solubility in common organic solvents that may facilitate heterogeneous catalysis and easy recycling. Their phase purities were confirmed by experimental powder X-ray diffractions in comparison with simulated ones, as shown in Figure S1.

Single-crystal X-ray diffraction indicated that complex $\{[Cu_7(DSDC)_2(OH)_6(H_2O)_{10}]\cdot xH_2O\}_n$ (**1**) crystallizes in the trigonal space group $R\overline{3}$ (Table 1). Each asymmetric unit is constituted by three and a half Cu(II) cations, one tetraanionic $DSDC^{4-}$ ligand, three bridging hydroxyl groups, and five aqua ligands. The $DSDC^{4-}$ ligand bridges four Cu(II) cations by four distinct carboxylate oxygen atoms while both sulfonate groups of the ligand remain free from metal coordination (Figure 1a). All Cu(II) cations are six-coordinated and bind with carboxylate oxygens, μ_3-bridging hydroxyl groups, and μ_2-bridging or terminal aqua ligands to form distorted octahedral coordination geometries. As a result, the nonlinear O−Cu−O angles fall in the range 79.70(13)−106.18(14)° for all symmetry-independent Cu(II) cations. The equatorial Cu−O bond lengths are between 1.914(3) and 2.007(3) Å [1.914(3)−1.974(4) Å for Cu1; 1.944(3)−1.981(3) Å for Cu2; 1.917(3)−1.988(4) Å for Cu3; 1.964(3)−2.007(3) Å for Cu4] while the axial Cu−O distances range from 2.437(4) to 2.617(4) Å [2.437(4)/2.617(4) Å for Cu1; 2.433(4)/2.590(4) Å for Cu2; 2.448(4)/2.521(4) Å for Cu3; 2.495(3)/2.495(3) Å for Cu4]. Significant elongation of the axial Cu−O bond lengths has been observed for all Cu(II) centers due to the Jahn−Teller effect, which exists widely in copper-based coordination complexes.

A disclike centrosymmetric heptanuclear $[Cu_7(\mu_3\text{-}OH)_6(H_2O)_{10}]^{8+}$ (**7Cu**) cluster could be identified in the structure of complex **1**, in which the Cu4 atom locates on the inversion center, as shown in Figure 1a. The central Cu4 atom is homocoordinated to six hydroxyl groups. The Cu···Cu separations in the **7Cu** cluster range from 3.0222(7) to 3.2143(7) Å and $Cu{-}O_{hydroxyl/water}{-}Cu$ angles are between 92.44(12) and 116.17(16)°. The mean atomic deviation is 0.0336 Å of the plane constituted by seven Cu(II) cations in the **7Cu** cluster. Each **7Cu** cluster is supported by four $DSDC^{4-}$ ligands, which further bridge the **7Cu** clusters into a three-dimensional framework (Figure 1b). From a topological point of view, each **7Cu** cluster as the secondary building unit (SBU) constitutes a four-connected node surrounded by four $DSDC^{4-}$ ligands and each $DSDC^{4-}$ ligands bridges two neighboring **7Cu** SBU. Therefore, a NbO type topology can be induced for the framework, whose Schäfli notation is expressed as $(6^4\cdot 8^2)$ (Figure 1c). The framework contains a one-dimensional hexagonal channel extending along the [001] direction, with a diameter of around 11 Å. Uncoordinated sulfonate groups and terminal aqua ligands protrude into the channels, interacting with guest water molecules via versatile hydrogen bonding.

Complex $\{[Cu_4(DSDC)(4,4'\text{-bpy})_2(OH)_4]\cdot 2H_2O\}_n$ (**2**) crystallizes in monoclinic space group $C2/c$, bearing an asymmetrical unit constituted by two symmetry-independent Cu(II) cations, half of a $DSDC^{4-}$ ligand, two hydroxyl groups, one 4,4′-bpy, and a lattice water molecule. Two carboxylate O atoms, three hydroxyl groups, and one pyridyl N atom account for the distorted octahedral coordination geometry of Cu1, whereas the Cu2 center adopts a pyramidal coordination environment consisting of one sulfonate O atom, three hydroxyl groups, and one pyridyl N atom. The nonlinear O−Cu−O angles are between 79.08(8) and 106.15(8) Å for Cu1 and 84.02(9) and 101.53(9) Å for Cu2, indicating that coordination geometries of both metal centers are significantly distorted. The Cu−O bond lengths vary in the range 1.934(2)−2.620(2) Å for Cu1 and 1.946(2)−2.288(2) Å for Cu2, and Cu−N distances are 2.001(2) Å for Cu1 and 2.028(2) Å for Cu2. Notably, the Jahn−Teller effect is also observed in the metal coordination of complex **2**, leading to obvious longer Cu−O bond lengths in the axial direction. Each $DSDC^{4-}$ ligand takes the μ_6-coordination mode utilizing all four carboxylate O atoms and two sulfonate O atoms, interconnecting six Cu(II) atoms. Adjacent symmetry−independent Cu(II) atoms are bridged by hydroxyl groups to form a waving $\{[Cu_2(OH)_2]^{2+}\}_n$ ladderlike belt (Figure 2a). The belt is also supported by alternate coordination of the $DSDC^{4-}$ ligand through its carboxylate groups. The one-dimensional belts are further assembled together into a three-dimensional framework through the coordination linkage of $DSDC^{4-}$ ligand using its sulfonate groups and auxiliary ligands (Figure 2b).

Complex $\{Cu_2(DSDC)(phen)_2(H_2O)_2\}_n$ (**3**) crystallizes in orthorhombic space group *Pccn* according to single-crystal X-ray

DOI: 10.1021/acs.inorgchem.9b02084
Inorg. Chem. XXXX, XXX, XXX−XXX

analysis (Table 1). With two symmetry-independent Cu(II) cations, one DSDC^{4-} ligand, two 1,10-phenanthroline, and two aqua ligands in the asymmetric unit, complex **3** features a two-dimensional infinite network. There are two types of Cu(II) centers with different coordination geometries, bound by two symmetry independent phenanthroline ligands. Cu1 binds to a pair of O atoms from two carboxylate groups of the same DSDC^{4-} ligands, one sulfonate O atom from another symmetry related DSDC^{4-} ligand, one aqua ligand, and two N atoms of a single phenanthroline ligand, leading to a distorted octahedral geometry as reflected by nonlinear O/N−Cu1−O/N bond angles between 81.25(8) and 102.89(8) ° (Figure 3a). The equatorial Cu1−O/N bond lengths fall in the range 1.962(2)−2.016(2) Å, and the axial Cu1−O distances are 2.459(2) and 2.491(2) Å due to the Jahn−Teller effect. Cu2 adopts pyramidal coordination geometry, with four basic corners occupied by two N atoms of a second phenanthroline ligand, one carboxylate O atom, and one aqua ligand. A sulfonate O atom locates at the apex of the pyramid at elongated bond distances of 2.219(2) Å due to the Jahn−Teller effect (Figure 3a). The Cu2−O/N bond lengths between 1.937(2) and 2.219(2) Å and the nonlinear O/N−Cu2−O/N bond angles between 82.18(10) and 105.65(9)° suggest a distorted pyramid. The DSDC^{4-} ligand bridges four Cu(II) cations with all carboxylate and sulfonate groups involved in coordination. Both sulfonate groups bind to distinct Cu(II) cations in monodentate mode, and two carboxylate groups chelate with one Cu(II) cation, one of which also coordinates to another Cu(II) cation using an alternate O atom. As a typical terminal ligand, the 1,10-phenanthroline precludes the formation of the three-dimensional framework; thus, the metal−organic coordination in this complex leads to only a two-dimensional network spreading over the (010) plane (Figure 3b).

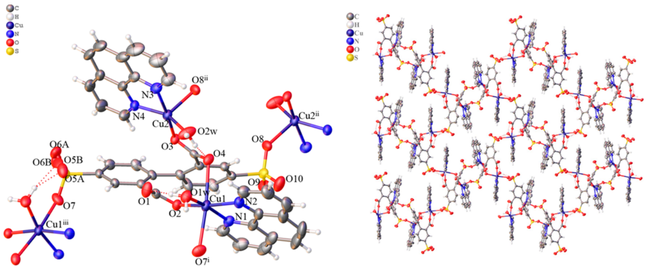

(a) (b)

Figure 3. (a) Coordination geometries of Cu(II) centers and binding mode of the ligand in complex **3**. (b) Two-dimensional layered structure in complex **3**. Symmetric codes: ^{i} 1/2 − *x*, +*y*, 1/2 + *z*; ^{ii} 1 − *x*, 1 − *y*, 1 − *z*; ^{iii} 1/2 − *x*, +*y*, −1/2 + *z*.

Versatile coordination groups in the designed DSDC^{4-} ligand dictate rich potential coordination modes, which may lead to various polymeric complexes (Table 2). All three Cu(II) complexes thus synthesized are revealed to be polymeric according to X-ray single-crystal structure analyses, demonstrating poor solubility in common solvents such as water, acetonitrile, acetone, methanol, dichloromethane, tetrahydrofuran, and toluene, which may facilitate heterogeneous catalysis and easy recycling.

Photocatalytic Studies. Guided by the objective of developing new photocatalysts, all complexes were subjected to the evaluation of their catalytic activities toward the oxidation of alcohols irradiated by visible light. The oxidation of alcohols to the corresponding carbonyl compounds is a critical transformation in organic synthesis.[53−58] Many catalytic systems, homogeneous or heterogeneous, have been developed for the oxidation of alcohols, forming corresponding aldehydes, carboxylic acids, or esters depending on the level of oxidation and esterification, with poor or satisfactory yields depending on the catalytic system.[29,53,59−61] Despite the progresses made toward this end, available catalysts are still limited with versatile disadvantages, such as the need of harsh reaction conditions, the involvement of noble or toxic metals, the use of costly cocatalysts, and poor recyclability.[62−64] To the best of our knowledge, there are no attempts utilizing visible light to mediate the oxidation reaction. The development of a photocatalytic system utilizing a highly efficient heterogeneous catalyst with good recyclability is of great importance in terms of green chemistry.[65−67]

The study began with the survey and optimization of reaction conditions. With benzyl alcohol as the substrate, reaction conditions with varied factors including photocatalysts, solvents, oxidant, and visible light have been systematically investigated. An initial study revealed that the ligand itself did not catalyze the reaction (Table 3, entry 1). Acetonitrile was found to be the best solvent to mediate this reaction (Table 3, entries 2−3). Other solvents giving poor yields and product selectivity were not listed. No occurrence of any reactions was observed with the absence of either blue LED or oxidant (Table 3, entries 4−5).

Table 2. Coordination Modes of DSDC^{4-} Ligand in Complexes 1−3 and Key Structural Parameters Defining the Ligand Conformations

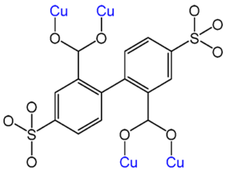

1

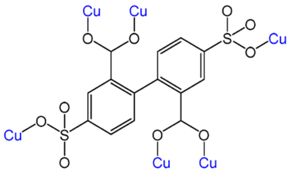

2

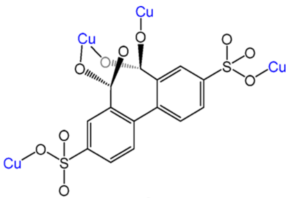

3

	distance between the two carboxylate C atoms (Å)	dihedral angles (deg)			
		between phenyl rings	carboxylate group vs attached benzyl ring		carboxylate group vs carboxylate group
1	4.00	85.5	31.9	41.9	78.6
2	4.67	73.1	21.3	21.3	89.4
3	2.93	48.5	31.9	42.3	18.5

Table 3. Optimization of Reaction Conditions[a]

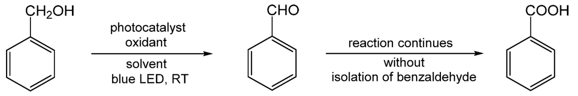

entry	photocatalyst (mol %)	solvent	visible light	oxidant	product and yield (%, isolation/in situ)	
					PhCHO (at 24 h)	PhCOOH (at 60 h)
1	H_4DSDC (10)	MeCN	blue LED	H_2O_2	–	–
2	**1** (10)	MeCN	blue LED	H_2O_2	74/85	88/90
3	**1** (10)	MeOH	blue LED	H_2O_2	45/55	53/56
4	**1** (10)	MeCN	–	H_2O_2	–	–
5	**1** (10)	MeCN	blue LED	–	–	–
6	**1** (10)	MeCN	blue LED	O_2	trace	trace
7	**1** (5)	MeCN	blue LED	H_2O_2	66/76	78/80
8	**2** (10)	MeCN	blue LED	H_2O_2	–	41/45
9	**3** (10)	MeCN	blue LED	H_2O_2	–	23/25

[a]Some other reaction conditions: benzyl alcohol (0.4 mmol), H_2O_2 (1.2 mmol, wherever applied), solvent (2 mL), 20 W blue LED used (450–470 nm).

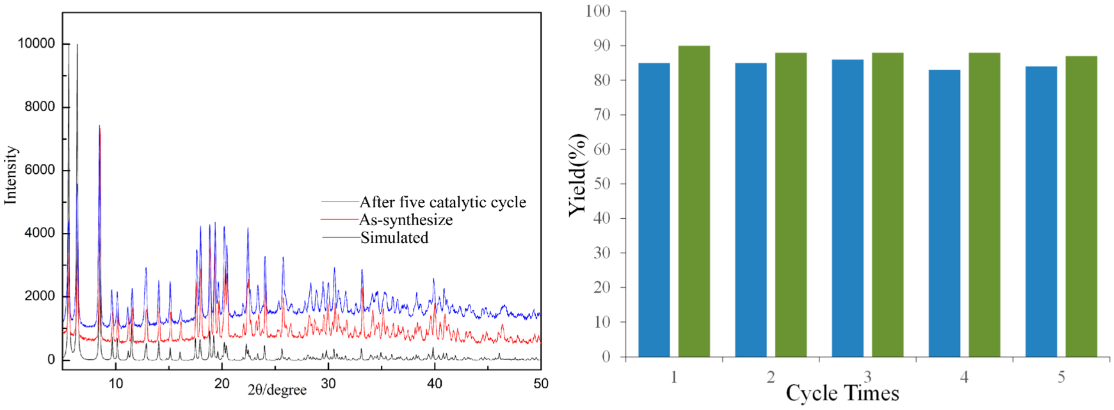

(a)

(b)

Figure 4. (a) Powder X-ray diffraction patterns of photocatalyst **1** before and after five catalytic recycles. (b) Recyclability of the photocatalyst **1**. The blue bar is the isolation yield of benzaldehyde at 24 h, and the green bar is the isolation yield of benzoic acid at 60 h for a separate run. All yields are based on parallel reactions.

When molecular oxygen was used as the oxidant, only a trace amount of product was observed (Table 3, entry 6). The minimum amount of photocatalyst required for a satisfactory yield was found to be 0.1 equiv (Table 3, entries 2 and 7). Therefore, the best reaction conditions for the photocatalytic oxidation of benzyl alcohol is the application of 10 mol % complex **1** as the photocatalyst, with H_2O_2 as the oxidant, and MeCN as the solvent, utilizing the irradiation of blue LED at room temperature (Table 3, entry 2).

Significantly for this photocatalytic system, the reaction exhibits stepwise oxidation to generate first benzaldehyde in the early stage and then benzoic acid with an elongated reaction time, fabricating a unique catalytic system with perfect time-resolved product selectivity. As shown by entry 2 in Table 1, after 24 h of reaction, benzaldehyde dominates the product with an isolation yield at 74% (85% in situ), while in a parallel run without the isolation of benzaldehyde, benzoic acid represents the major product at 88% isolation yield (90% in situ) after 60 h of reaction. A systematic investigation on the in situ yields of benzaldehyde and benzoic acid during reaction process have been carried out. The yield of benzaldehyde increases in the first 24 h of the reaction while very little benzoic acid is generated during this period. Then benzaldehyde starts to be oxidized further into benzoic acid, resulting in a decreasing amount of benzaldehyde and an increasing amount of benzoic acid (see Supporting Information for graphic representation and corresponding data regarding the time-resolved yields of the two products). To the best of our knowledge, this case represents the sole example that a catalyst shows time-resolved multistage selective catalysis for different products with satisfactory isolation yields.

Complexes **2** and **3** exhibited poor catalytic activity and no stepwise oxidation was observed (Table 3, entries 8 and 9), which is out of our expectation. Further studies revealed that the UV–vis absorption of complex **1** differs significantly from those of the ligand and complexes **2** and **3**, and this might be an explanation of the distinct catalytic properties for these complexes. The utilization of a bridging auxiliary ligand (4,4′-bipyridine) led to a less stable complex **2**, which compared to **1** is also less efficient in catalysis (Table 3, entries 2 and 8). The introduction of an auxiliary ligand (1,10-phenanthroline) capable of facilitating light absorption made no contribution to the catalytic activity of **3**, whose catalytic efficiency in promoting the reaction decreased dramatically compared to that of **1** (Table 3, entries 2 and 9). The use of auxiliary ligands might be able to enhance the physical property of the metal complexes

DOI: 10.1021/acs.inorgchem.9b02084
Inorg. Chem. XXXX, XXX, XXX–XXX

Table 4. Substrates Scope[a]

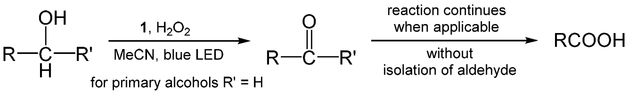

Entry	Substrates	Product and yield (%, isolation / in-situ)		Entry	Substrates	Product and isolation yield (%)
		RCHO	RCOOH			RC(O)R'
1	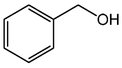	74 / 85	88 / 90	9	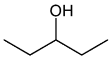	73
2	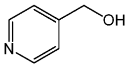	76 / 83	82 / 85	10	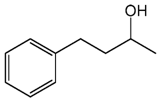	71
3	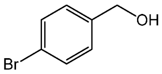	75 / 85	88 / 90	11	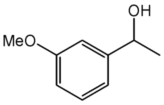	63
4	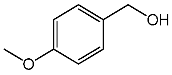	74 / 83	80 / 82	12	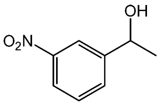	61
5	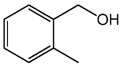	77 / 86	89 / 91	13	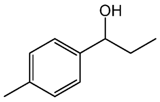	65
6	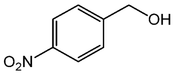	72 / 80	80 / 82			
7	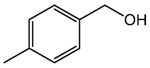	76 / 85	86 / 88			
8	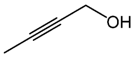	not observed	64 / 70			

[a] Note: Oxidation of aryl primary alcohols into aldehydes took 24 h and oxidation of secondary alcohols into ketones took 48 h. Reaction conditions (unless otherwise specified): primary alcohols (0.4 mmol), H_2O_2 (1.2 mmol), complex **1** (0.04 mmol), CH_3CN (2.0 mL), irradiated by 20 W blue LEDs (450 nm−470 nm) in air at room temperature.

in certain aspects, but this may not always contribute positively to the catalytic activity of the complex. Factors that might potentially affect the catalytic activities of these complexes in this photooxidation reaction include distinct porosities that may contribute substantially to selectivity and yield, different bulkiness of the auxiliary ligands that may block catalytic center, various intrinsic features of different Cu−O cluster moieties, and a potential synergetic effect between the $DSDC^{4-}$ ligand and Cu−O clusters. Further studies in this area may be able to provide more information in the future.

One of the remarkable features of this catalytic system is that photocatalyst **1** could be recovered almost quantitatively on completion of the reaction with the structure being intact. To determine possible metal leaching into the remaining solution on completion of the reaction, the reaction mixture was filtrated to remove the solid catalyst and the filtrate was subjected to an analysis using inductively coupled plasma atomic emission spectroscopy. The result indicated that the concentration of Cu element in the filtrate was 0.01 $\mu g \cdot mL^{-1}$, which accounts for a 0.00286‰ loss of the catalyst, suggesting negligible metal leaching, which provides a perfect recovery rate and the possibility of catalyst recycling.

The recyclability and reusability of complex **1** as a catalyst in this reaction were then evaluated with benzyl alcohol as the substrate. After each reaction cycle (60 h without the isolation of benzaldehyde), photocatalyst **1** was isolated by filtration, washed with acetone, dried in vacuum, and subjected to recycled use in another catalytic cycle without any need of activation or regeneration. A series of paralleled runs revealed that after five catalytic cycles, photocatalyst **1** remains unchanged according to almost constant powder XRD patterns and IR spectra before and after catalysis (Figure 4a and Figure S3), and most importantly there was no obvious dropping of the catalytic efficiency (Figure 4b).

The substrate scope of the oxidation reaction was then investigated with both primary and secondary alcohols, as shown in Table 4. For primary alcohols with different aromatic functional groups, no matter if it was a phenyl ring with either an electron withdrawing or electron donating group or even if it was a heterocyclic ring, all these substrates exhibited good adaptability over this oxidation reaction using complex **1** as the photocatalyst, giving corresponding aldehydes or carboxylic acids in good yields (Table 4, entries 1−7). The photocatalyst showed perfect compatibility with selective time-resolved control and constant recyclability upon reactions of these substrates. When the aliphatic primary alcohol was subjected to this photocatalytic reaction, no stepwise oxidation was observed and only the corresponding carboxylate acid was isolated in medium yield (Table 4, entry 8). Regarding the secondary alcohols, a direct oxidation into ketones occurred with satisfactory yields (Table 4, entries 9−13).

■ CONCLUSIONS

A family of three coordination polymers comprising various Cu−O assemblies has been synthesized, which can be used as heterogeneous photocatalysts for the visible-light driven oxidation reactions of alcohols. Complex **1** exhibits the best catalytic efficiency, which is constituted by the infinite linkage of heptanuclear $[Cu_7(\mu_3\text{-}OH)_6(H_2O)_{10}]^{8+}$ clusters via deprotonated $DSDC^{4-}$ ligands into a NbO type topology. The reaction conditions required for this catalytic system are environment friendly, such as the use of visible light (blue LED) at room temperature, the application of hydrogen peroxide as an oxidant, easy isolation and recyclability of the catalyst, etc.

With primary aryl alcohols as the reaction substrate, different oxidation products of aldehydes or carboxylic acids could be generated at different stages of the catalytic reaction and could be isolated in good yield, constituting a unique example of stepwise catalysis with perfect time-resolved control. Significantly, this MOF photocatalyst **1** could be quantitatively recovered as a crystalline material with negligible metal leaching on completion of the reaction, being structurally unchanged and recyclable for at least five catalytic cycles with constant efficiency and consistent activity of stepwise catalysis. This Cu-based MOF **1** represents the first example of a photocatalyst capable of catalyzing successive reactions with good time-resolved control of products. According to the reaction process, it is possible to design a flow reactor toward low-cost large-scale production on the basis of the efficiency and recyclability of the photocatalyst. This novel catalytic system of stepwise catalysis with good multistage selectivity gives new insight into the design and development of new types of catalysts for both fundamental studies and industrial uses toward challenging organic transformations.

■ ASSOCIATED CONTENT

Ⓢ Supporting Information

The Supporting Information is available free of charge at https://pubs.acs.org/doi/10.1021/acs.inorgchem.9b02084.

> PXRD data (Figure S1), TGA curves (Figure S2), IR spectra of complex **1** before and after catalysis (Figure S3), time-resolved yields comparison (Table S1 and Figure S4), UV−vis spectra (Figure S5), selected bond lengths and angles (Table S2), product yields and NMR spectra (PDF)

Accession Codes

CCDC 1903006−1903008 contain the supplementary crystallographic data for this paper. These data can be obtained free of charge via www.ccdc.cam.ac.uk/data_request/cif, or by emailing data_request@ccdc.cam.ac.uk, or by contacting The Cambridge Crystallographic Data Centre, 12 Union Road, Cambridge CB2 1EZ, UK; fax: +44 1223 336033.

■ AUTHOR INFORMATION

Corresponding Authors

*Email: xlzhao@chem.ecnu.edu.cn (X.L.Z.).
*Email: xdchen@njnu.edu.cn (X.D.C.).

ORCID

Jie Zhou: 0000-0002-0769-2543
Xiao-Li Zhao: 0000-0002-4458-6432
Xu-Dong Chen: 0000-0002-0152-5410

Notes

The authors declare no competing financial interest.

■ ACKNOWLEDGMENTS

This work was supported by the National Natural Science Foundation of China (21671104), the Jiangsu Key Technology R&D Program (BE2016010 and BE2016010-1), the Natural Science Foundation of Jiangsu Higher Education Institutions of China (17KJA430010 and 15KJA350002), the Priority Academic Program Development of Jiangsu Higher Educational Institutions, the Jiangsu Collaborative Innovation Center of Biomedical Functional Materials, and the State Key Laboratory of Coordination Chemistry in Nanjing University. We thank the staff of the BL17B beamline of the National Facility for Protein Science Shanghai (NFPS) at the Shanghai Synchrotron Radiation Facility (SSRF).

■ REFERENCES

(1) Joarder, B.; Lin, J. B.; Romero, Z.; Shimizu, G. K. H. Single Crystal Proton Conduction Study of a Metal Organic Framework of Modest Water Stability. *J. Am. Chem. Soc.* **2017**, *139*, 7176−7179.

(2) Yamada, T.; Otsubo, K.; Makiura, R.; Kitagawa, H. Designer coordination polymers: dimensional crossover architectures and proton conduction. *Chem. Soc. Rev.* **2013**, *42*, 6655−6669.

(3) Ramaswamy, P.; Wong, N. E.; Shimizu, G. K. MOFs as proton conductors–challenges and opportunities. *Chem. Soc. Rev.* **2014**, *43*, 5913−32.

(4) Ye, Y.; Guo, W.; Wang, L.; Li, Z.; Song, Z.; Chen, J.; Zhang, Z.; Xiang, S.; Chen, B. Straightforward Loading of Imidazole Molecules into Metal-Organic Framework for High Proton Conduction. *J. Am. Chem. Soc.* **2017**, *139*, 15604−15607.

(5) Zhang, F. M.; Dong, L. Z.; Qin, J. S.; Guan, W.; Liu, J.; Li, S. L.; Lu, M.; Lan, Y. Q.; Su, Z. M.; Zhou, H. C. Effect of Imidazole Arrangements on Proton-Conductivity in Metal-Organic Frameworks. *J. Am. Chem. Soc.* **2017**, *139*, 6183−6189.

(6) Bunzen, H.; Kolbe, F.; Kalytta-Mewes, A.; Sastre, G.; Brunner, E.; Volkmer, D. 6 Achieving Large Volumetric Gas Storage Capacity in Metal-Organic Frameworks by Kinetic Trapping: A Case Study of Xenon Loading in MFU-4. *J. Am. Chem. Soc.* **2018**, *140*, 10191−10197.

(7) Alezi, D.; Belmabkhout, Y.; Suyetin, M.; Bhatt, P. M.; Weselinski, L. J.; Solovyeva, V.; Adil, K.; Spanopoulos, I.; Trikalitis, P. N.; Emwas, A. H.; Eddaoudi, M. MOF Crystal Chemistry Paving the Way to Gas Storage Needs: Aluminum-Based soc-MOF for CH_4, O_2, and CO_2 Storage. *J. Am. Chem. Soc.* **2015**, *137*, 13308−13318.

(8) Yan, Y.; Kolokolov, D. I.; da Silva, I.; Stepanov, A. G.; Blake, A. J.; Dailly, A.; Manuel, P.; Tang, C. C.; Yang, S.; Schroder, M. Porous Metal-Organic Polyhedral Frameworks with Optimal Molecular Dynamics and Pore Geometry for Methane Storage. *J. Am. Chem. Soc.* **2017**, *139*, 13349−13360.

(9) He, Y.; Zhou, W.; Qian, G.; Chen, B. Methane storage in metal-organic frameworks. *Chem. Soc. Rev.* **2014**, *43*, 5657−5678.

(10) Godfrey, H. G. W.; da Silva, I.; Briggs, L.; Carter, J. H.; Morris, C. G.; Savage, M.; Easun, T. L.; Manuel, P.; Murray, C. A.; Tang, C. C.; Frogley, M. D.; Cinque, G.; Yang, S.; Schröder, M. Ammonia Storage by Reversible Host−Guest Site Exchange in a Robust Metal−Organic Framework. *Angew. Chem., Int. Ed.* **2018**, *57*, 14778−14781.

(11) Cadiau, A.; Belmabkhout, Y.; Adil, K.; Bhatt, P. M.; Pillai, R. S.; Shkurenko, A.; Martineau-Corcos, C.; Maurin, G.; Eddaoudi, M. Hydrolytically stable fluorinated metal-organic frameworks for energy-efficient dehydration. *Science* **2017**, *356*, 731−735.

(12) Gascon, J. Flicking the switch on a molecular gate. *Science* **2017**, *358*, 303.

(13) Liao, P.-Q.; Huang, N.-Y.; Zhang, W.-X.; Zhang, J.-P.; Chen, X.-M. Controlling guest conformation for efficient purification of butadiene. *Science* **2017**, *356*, 1193−1196.

(14) Li, L.; Lin, R.-B.; Krishna, R.; Li, H.; Xiang, S.; Wu, H.; Li, J.; Zhou, W.; Chen, B. Ethane/ethylene separation in a metal-organic framework with iron-peroxo sites. *Science* **2018**, *362*, 443−446.

(15) Cui, X.; Chen, K.; Xing, H.; Yang, Q.; Krishna, R.; Bao, Z.; Wu, H.; Zhou, W.; Dong, X.; Han, Y.; Li, B.; Ren, Q.; Zaworotko, M. J.; Chen, B. Pore chemistry and size control in hybrid porous materials for acetylene capture from ethylene. *Science* **2016**, *353*, 141−144.

(16) Cadiau, A.; Adil, K.; Bhatt, P. M.; Belmabkhout, Y.; Eddaoudi, M. A metal-organic framework−based splitter for separating propylene from propane. *Science* **2016**, *353*, 137−140.

(17) Gu, C.; Hosono, N.; Zheng, J.-J.; Sato, Y.; Kusaka, S.; Sakaki, S.; Kitagawa, S. Design and control of gas diffusion process in a nanoporous soft crystal. *Science* **2019**, *363*, 387−391.

(18) Adil, K.; Belmabkhout, Y.; Pillai, R. S.; Cadiau, A.; Bhatt, P. M.; Assen, A. H.; Maurin, G.; Eddaoudi, M. Gas/vapour separation using ultra-microporous metal-organic frameworks: insights into the structure/separation relationship. *Chem. Soc. Rev.* **2017**, *46*, 3402−3430.

(19) Liu, S.-Y.; Zhou, D.-D.; He, C.-T.; Liao, P.-Q.; Cheng, X.-N.; Xu, Y.-T.; Ye, J.-W.; Zhang, J.-P.; Chen, X.-M. Flexible, Luminescent Metal−Organic Frameworks Showing Synergistic Solid-Solution Effects on Porosity and Sensitivity. *Angew. Chem., Int. Ed.* **2016**, *55*, 16021−16025.

(20) Huang, R. W.; Wei, Y. S.; Dong, X. Y.; Wu, X. H.; Du, C. X.; Zang, S. Q.; Mak, T. C. W. Hypersensitive dual-function luminescence switching of a silver-chalcogenolate cluster-based metal-organic framework. *Nat. Chem.* **2017**, *9*, 689−697.

(21) Wang, H.-S.; Li, J.; Li, J.-Y.; Wang, K.; Ding, Y.; Xia, X.-H. Lanthanide-based metal-organic framework nanosheets with unique fluorescence quenching properties for two-color intracellular adenosine imaging in living cells. *NPG Asia Mater.* **2017**, *9*, No. e354.

(22) Xu, X. Y.; Lian, X.; Hao, J. N.; Zhang, C.; Yan, B. A Double-Stimuli-Responsive Fluorescent Center for Monitoring of Food Spoilage based on Dye Covalently Modified EuMOFs: From Sensory Hydrogels to Logic Devices. *Adv. Mater.* **2017**, *29*, 1702298.

(23) He, T.; Chen, S.; Ni, B.; Gong, Y.; Wu, Z.; Song, L.; Gu, L.; Hu, W.; Wang, X. Zirconium-Porphyrin-Based Metal-Organic Framework Hollow Nanotubes for Immobilization of Noble-Metal Single Atoms. *Angew. Chem., Int. Ed.* **2018**, *57*, 3493−3498.

(24) Dhakshinamoorthy, A.; Li, Z.; Garcia, H. Catalysis and photocatalysis by metal organic frameworks. *Chem. Soc. Rev.* **2018**, *47*, 8134−8172.

(25) Zhu, L.; Liu, X. Q.; Jiang, H. L.; Sun, L. B. Metal-Organic Frameworks for Heterogeneous Basic Catalysis. *Chem. Rev.* **2017**, *117*, 8129−8176.

(26) Liu, J.; Chen, L.; Cui, H.; Zhang, J.; Zhang, L.; Su, C. Y. Applications of metal-organic frameworks in heterogeneous supramolecular catalysis. *Chem. Soc. Rev.* **2014**, *43*, 6011−6061.

(27) Zhao, M.; Ou, S.; Wu, C. D. Porous metal-organic frameworks for heterogeneous biomimetic catalysis. *Acc. Chem. Res.* **2014**, *47*, 1199−1207.

(28) Yang, Q.; Xu, Q.; Jiang, H. L. Metal-organic frameworks meet metal nanoparticles: synergistic effect for enhanced catalysis. *Chem. Soc. Rev.* **2017**, *46*, 4774−4808.

(29) Xiao, J. D.; Jiang, H. L. Metal-Organic Frameworks for Photocatalysis and Photothermal Catalysis. *Acc. Chem. Res.* **2019**, *52*, 356−366.

(30) Fukuzumi, S.; Ohkubo, K. Selective photocatalytic reactions with organic photocatalysts. *Chem. Sci.* **2013**, *4*, 561−574.

(31) Yan, Z. H.; Du, M. H.; Liu, J.; Jin, S.; Wang, C.; Zhuang, G. L.; Kong, X. J.; Long, L. S.; Zheng, L. S. Photo-generated dinuclear $\{Eu(II)\}_2$ active sites for selective CO_2 reduction in a photosensitizing metal-organic framework. *Nat. Commun.* **2018**, *9*, 3353.

(32) Xiao, Y.; Qi, Y.; Wang, X.; Wang, X.; Zhang, F.; Li, C. Visible-Light-Responsive 2D Cadmium-Organic Framework Single Crystals with Dual Functions of Water Reduction and Oxidation. *Adv. Mater.* **2018**, *30*, No. e1803401.

(33) Happ, B.; Winter, A.; Hager, M. D.; Schubert, U. S. Photogenerated avenues in macromolecules containing Re(I), Ru(II), Os(II), and Ir(III) metal complexes of pyridine-based ligands. *Chem. Soc. Rev.* **2012**, *41*, 2222−2255.

(34) Yoon, T. P.; Ischay, M. A.; Du, J. Visible light photocatalysis as a greener approach to photochemical synthesis. *Nat. Chem.* **2010**, *2*, 527.

(35) Xuan, J.; Xiao, W. J. Visible-light photoredox catalysis. *Angew. Chem., Int. Ed.* **2012**, *51*, 6828−6838.

(36) Nicewicz, D. A.; Nguyen, T. M. Recent Applications of Organic Dyes as Photoredox Catalysts in Organic Synthesis. *ACS Catal.* **2014**, *4*, 355−360.

(37) Hari, D. P.; König, B. Synthetic applications of eosin Y in photoredox catalysis. *Chem. Commun.* **2014**, *50*, 6688−6699.

(38) Xiao, J. D.; Han, L.; Luo, J.; Yu, S. H.; Jiang, H. L. Integration of Plasmonic Effects and Schottky Junctions into Metal-Organic Framework Composites: Steering Charge Flow for Enhanced Visible-Light Photocatalysis. *Angew. Chem., Int. Ed.* **2018**, *57*, 1103−1107.

(39) Diercks, C. S.; Liu, Y.; Cordova, K. E.; Yaghi, O. M. The role of reticular chemistry in the design of CO_2 reduction catalysts. *Nat. Mater.* **2018**, *17*, 301−307.

(40) Ye, C. P.; Xu, G.; Wang, Z.; Han, J.; Xue, L.; Cao, F. Y.; Zhang, Q.; Yang, L. F.; Lin, L. Z.; Chen, X. D. Design and synthesis of functionalized coordination polymers as recyclable heterogeneous photocatalysts. *Dalton. Trans.* **2018**, *47*, 6470−6478.

(41) Kou, J.; Lu, C.; Wang, J.; Chen, Y.; Xu, Z.; Varma, R. S. Selectivity Enhancement in Heterogeneous Photocatalytic Transformations. *Chem. Rev.* **2017**, *117*, 1445−1514.

(42) Ikuno, T.; Zheng, J.; Vjunov, A.; Sanchez-Sanchez, M.; Ortuno, M. A.; Pahls, D. R.; Fulton, J. L.; Camaioni, D. M.; Li, Z.; Ray, D.; Mehdi, B. L.; Browning, N. D.; Farha, O. K.; Hupp, J. T.; Cramer, C. J.; Gagliardi, L.; Lercher, J. A. Methane Oxidation to Methanol Catalyzed by Cu-Oxo Clusters Stabilized in NU-1000 Metal-Organic Framework. *J. Am. Chem. Soc.* **2017**, *139*, 10294−10301.

(43) Jiang, X.; Li, J.; Yang, B.; Wei, X. Z.; Dong, B. W.; Kao, Y.; Huang, M. Y.; Tung, C. H.; Wu, L. Z. A Bio-inspired Cu_4O_4 Cubane: Effective Molecular Catalysts for Electrocatalytic Water Oxidation in Aqueous Solution. *Angew. Chem., Int. Ed.* **2018**, *57*, 7850−7854.

(44) Li, H. X.; Ren, Z. G.; Liu, D.; Chen, Y.; Lang, J. P.; Cheng, Z. P.; Zhu, X. L.; Abrahams, B. F. Single-crystal-to-single-crystal structural transformations of two sandwich-like Cu(II) pyrazolate complexes and their excellent catalytic performances in MMA polymerization. *Chem. Commun.* **2010**, *46*, 8430−8432.

(45) Liu, Z. Y.; Zhang, H. Y.; Yang, E. C.; Liu, Z. Y.; Zhao, X. J. A (3,6)-connected layer with an unprecedented adeninate nucleobase-derived heptanuclear disc. *Dalton. Trans.* **2015**, *44*, 5280−5283.

(46) Henkelis, J. J.; Jones, L. F.; de Miranda, M. P.; Kilner, C. A.; Halcrow, M. A. Two heptacopper(II) disk complexes with a $[Cu_7(\mu_3\text{-}OH)_4(\mu\text{-}OR)_2]^{8+}$ core. *Inorg. Chem.* **2010**, *49*, 11127−11132.

(47) Wang, X.; Chen, R. X.; Wei, Z. F.; Zhang, C. Y.; Tu, H. Y.; Zhang, A. D. Chemoselective transformation of diarylethanones to arylmethanoic acids and diarylmethanones and mechanistic insights. *J. Org. Chem.* **2016**, *81*, 238−249.

(48) Han, W.; Qin, S.; Shu, X.; Wu, Q.; Xu, B.; Li, R.; Zheng, X.; Chen, H. Synthesis of phosphorus amidite ligand and investigation of its flexibility impact on rhodium-catalyzed hydroformylation of 1-octene. *RSC Adv.* **2016**, *6*, 53012−53016.

(49) Sheldrick, G. *SADABS−Area Detector Scaling and Absorption*; Bruker AXS, 2008.

(50) Dolomanov, O. V.; Bourhis, L. J.; Gildea, R. J.; Howard, J. A. K.; Puschmann, H. OLEX2: a complete structure solution, refinement and analysis program. *J. Appl. Crystallogr.* **2009**, *42*, 339−341.

(51) Sheldrick, G. Crystal structure refinement with SHELXL. *Acta Crystallogr., Sect. C: Struct. Chem.* **2015**, *71*, 3−8.

(52) Sheldrick, G. SHELXT - Integrated space-group and crystal-structure determination. *Acta Crystallogr., Sect. A: Found. Adv.* **2015**, *71*, 3−8.

DOI: 10.1021/acs.inorgchem.9b02084
Inorg. Chem. XXXX, XXX, XXX−XXX

(53) Dai, Y.; Ren, P.; Li, Y.; Lv, D.; Shen, Y.; Li, Y.; Niemantsverdriet, H.; Besenbacher, F.; Xiang, H.; Hao, W.; Lock, N.; Wen, X.; Lewis, J. P.; Su, R. Solid Base $Bi_{24}O_{31}Br_{10}(OH)_\delta$ with Active Lattice Oxygen for Efficient Photo-oxidation of Primary Alcohols to Aldehydes. *Angew. Chem., Int. Ed.* **2019**, *58*, 1−7.

(54) Huang, W.; Ma, B. C.; Lu, H.; Li, R.; Wang, L.; Landfester, K.; Zhang, K. A. I. Visible-Light-Promoted Selective Oxidation of Alcohols Using a Covalent Triazine Framework. *ACS Catal.* **2017**, *7*, 5438−5442.

(55) Su, F.; Mathew, S. C.; Lipner, G.; Fu, X.; Antonietti, M.; Blechert, S.; Wang, X. mpg-C_3N_4-Catalyzed Selective Oxidation of Alcohols Using O_2 and Visible Light. *J. Am. Chem. Soc.* **2010**, *132*, 16299−16301.

(56) Hoover, J. M.; Stahl, S. S. Highly practical copper(I)/TEMPO catalyst system for chemoselective aerobic oxidation of primary alcohols. *J. Am. Chem. Soc.* **2011**, *133*, 16901−16910.

(57) Liang, S.; Wen, L.; Lin, S.; Bi, J.; Feng, P.; Fu, X.; Wu, L. Monolayer HNb_3O_8 for selective photocatalytic oxidation of benzylic alcohols with visible light response. *Angew. Chem., Int. Ed.* **2014**, *53*, 2951−5.

(58) Zhao, L. M.; Meng, Q. Y.; Fan, X. B.; Ye, C.; Li, X. B.; Chen, B.; Ramamurthy, V.; Tung, C. H.; Wu, L. Z. Photocatalysis with Quantum Dots and Visible Light: Selective and Efficient Oxidation of Alcohols to Carbonyl Compounds through a Radical Relay Process in Water. *Angew. Chem., Int. Ed.* **2017**, *56*, 3020−3024.

(59) Zhao, G.; Yang, F.; Chen, Z.; Liu, Q.; Ji, Y.; Zhang, Y.; Niu, Z.; Mao, J.; Bao, X.; Hu, P.; Li, Y. Metal/oxide interfacial effects on the selective oxidation of primary alcohols. *Nat. Commun.* **2017**, *8*, 14039.

(60) Mannel, D. S.; King, J.; Preger, Y.; Ahmed, M. S.; Root, T. W.; Stahl, S. S. Mechanistic Insights into Aerobic Oxidative Methyl Esterification of Primary Alcohols with Heterogeneous PdBiTe Catalysts. *ACS Catal.* **2018**, *8*, 1038−1047.

(61) Zhao, G.-m.; Liu, H.-l.; Zhang, D.-d.; Huang, X.-r.; Yang, X. DFT Study on Mechanism of N-alkylation of amino derivatives with primary alcohols catalyzed by copper(II) acetate. *ACS Catal.* **2014**, *4*, 2231−2240.

(62) Shirase, S.; Shinohara, K.; Tsurugi, H.; Mashima, K. Oxidation of alcohols to carbonyl compounds catalyzed by oxo-bridged dinuclear cerium complexes with pentadentate schiff-base ligands under a dioxygen atmosphere. *ACS Catal.* **2018**, *8*, 6939−6947.

(63) Cherepakhin, V.; Williams, T. J. Iridium catalysts for acceptorless dehydrogenation of alcohols to carboxylic acids: scope and mechanism. *ACS Catal.* **2018**, *8*, 3754−3763.

(64) Xu, B.; Lumb, J. P.; Arndtsen, B. A. A TEMPO-free copper-catalyzed aerobic oxidation of alcohols. *Angew. Chem., Int. Ed.* **2015**, *54*, 4208−4211.

(65) Schwarz, J.; Konig, B. Visible-light mediated C-C bond cleavage of 1,2-diols to carbonyls by cerium-photocatalysis. *Chem. Commun.* **2019**, *55*, 486−488.

(66) Li, H.; Yang, Y.; He, C.; Zeng, L.; Duan, C. Mixed-ligand metal−organic framework for two-photon responsive photocatalytic C−N and C−C coupling reactions. *ACS Catal.* **2019**, *9*, 422−430.

(67) Li, F. C.; Li, X. L.; Tan, L. K.; Wang, J. T.; Yao, W. Z. Evans-Showell-type polyoxometalate-based metal-organic complexes with novel 3D structures constructed from flexible bis-pyrazine-bis-amide ligands and copper metals: syntheses, structures, and fluorescence and catalytic properties. *Dalton. Trans.* **2019**, *48*, 2160−2169.

DOI: 10.1021/acs.inorgchem.9b02084
Inorg. Chem. XXXX, XXX, XXX−XXX